The development of dielectric barrier discharges in gas gaps and on surfaces

J. Phys. D: Appl. Phys. **33** (2000) 2618–2636. Printed in the UK PII: S0022-3727(00)13567-3

The development of dielectric barrier discharges in gas gaps and on surfaces

Valentin I Gibalov† and Gerhard J Pietsch‡

† Moscow State University, Department of Chemistry, Leninskie Gory, Moscow 119899, Russia
‡ Aachen University of Technology, Gasentladungstechnik, D-52056 Aachen, Germany

E-mail: pietsch@hst.rwth-aachen.de and gibalov@valentin.chem.msu.su

Received 27 April 2000, in final form 11 August 2000

Abstract. Dielectric barrier discharges (DBDs) occur in configurations which are characterized by a dielectric layer between conducting electrodes. Two basic configurations can be distinguished: a volume discharge (VD) arrangement with a gas gap; and a surface discharge (SD) arrangement with surface electrode(s) on a dielectric layer and an extensive counter electrode on its reverse side. At atmospheric pressure the DBD consists of numerous microdischarges (VD) and discharge steps (SD), respectively, their number being proportional to the amplitude of the voltage. These events have a short duration in the range of some 10 ns transferring a certain amount of charge within the discharge region. The total transferred charge determines the current and hence the volt–ampere characteristic of each arrangement. The microdischarges (discharge steps) have a complicated spatial structure. The discharge patterns on the dielectric surface depend on the polarity and amplitude of the applied voltage as well as on the specific capacity of the dielectric. Experimental findings on DBDs in air and oxygen are presented and discussed.

On the basis of a self-consistent two-dimensional modelling the temporal and spatial development of a microdischarge and discharge step are investigated numerically. The results lead to an understanding of the dynamics of DBDs. Although in VD arrangements cathode-directed streamers appear especially in electronegative gases, their appearance is rather unlikely in SD arrangements.

The application of DBDs for plasma–chemical reactions is determined by the productivity, with which the energy of the electric field can be converted into internal states of atoms and/or molecules. Depending on the desired product it could be both the generation of internal electronic states of molecules or atoms and dissociation products of molecules. The discharge current and current density of DBDs in both the SD and VD arrangements as well as the energy release and energy density distribution in the discharge region are presented. As an example the effectiveness of the energy conversion into ozone production is detailed. Some peculiarities of the discharge parameters, for instance the correlation between discharge patterns (microdischarges or discharge steps) and surface charge density, are discussed.

1. Introduction

If an ac voltage is applied to an electrode system with one or both electrodes covered by a dielectric layer, a dielectric barrier discharge (DBD) will appear in the gas gap. The DBD is a highly transient, low-temperature non-equilibrium discharge formed from electrons of high mean energy which exists in a broad range of pressures. During its development charge carriers collect on the dielectric(s) reducing the field strength in the discharge area and hence quenching the discharge. The high-energy electrons are effective in the generation of activated species and radicals. This type of discharge offers a wide field of applications, e.g. treatment of surfaces, mercury-free radiation sources and in plasma chemistry.

There are two basic configurations for generating DBDs. The first is the 'volume discharge' (VD) arrangement consisting, for example, of two parallel plates (figure 1(a)). The second is the 'surface discharge' (SD) arrangement, a plane dielectric with an electrode on one surface and a metallic cover on its reverse side (figure 1(b)). There are many possible combinations of these basic configurations; for example, some of them are found in plasma display panels (for the basics see figure 1(c)) or in some plasma chemical reactors (figure 1(d)). In both basic configurations the DBD consists of discharge pulses with a duration of about 10 ns at around atmospheric pressure depending on the boundary conditions.

While the DBD in VD arrangements has been investigated intensively, (e.g. [1–7]), investigations of SDs are scarce [8–11]. Much knowledge on DBDs is accumulated in [12]; a more recent review of the state of the art of DBDs and their applications is given in [13].

0022-3727/00/202618+19$30.00

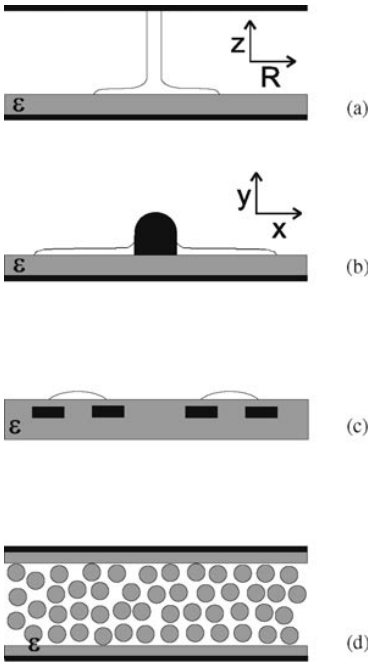

Figure 1. Basic configuration of (a) the volume discharge (VD), (b) the surface discharge (SD) plus combinations of them in (c) a coplanar arrangement and (d) a packed bed reactor (in black, metallic electrodes).

Numerical simulation of the dynamics of DBDs means, first of all, describing the spatial and temporal development of distinct microdischarges (VD) and single-discharge steps in thin layers on the dielectric surface (SD), respectively.

In VD arrangements the discharge channels are axially symmetric; in SD arrangements it is a good approach to take the discharge to be homogeneous along the surface electrode. This is why two-dimensional modelling is sufficient in both cases.

For the pre-given conditions (an approximate atmospheric gas pressure, an electrode gap distance of about a few millimetres and molecular gas mixtures) the swarm parameters describing the development of the discharge can be determined by the local field strength in general (local field approximation [14]).

As the DBD is a non-thermal transient discharge, even at atmospheric pressure there exists a considerable difference in the mean energy of the electrons and that of the heavy particles. This is why the energy of the electrons can be transformed into internal states of particles effectively. This effectiveness is affected by the energy released in the discharge as well as the dynamics of the energy transformation.

All results presented belong to DBD configurations and operating conditions which are typically for ozone generation. The discharge gap is less than 3 mm in the VD arrangements, the thickness of the dielectric is between 0.5 and 3 mm, and the relative permittivity ε_r is less than 50. The process gas is air or oxygen at around atmospheric pressure, the frequency of the applied voltage goes up to several kHz. Most of the results, however, are not limited to these specific conditions.

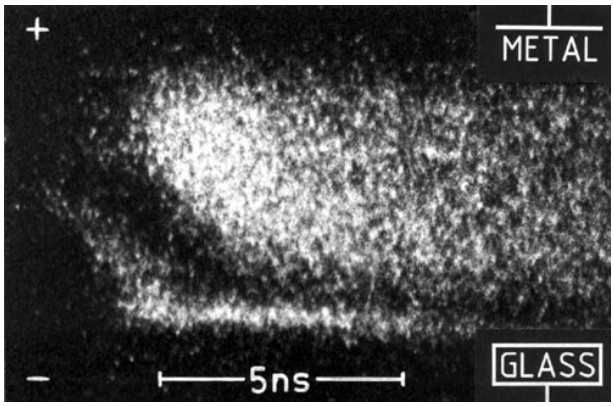

Figure 2. A streak photograph of a microdischarge in a VD arrangement (in the visible spectrum range; air at atmospheric pressure, 4 mm gap distance).

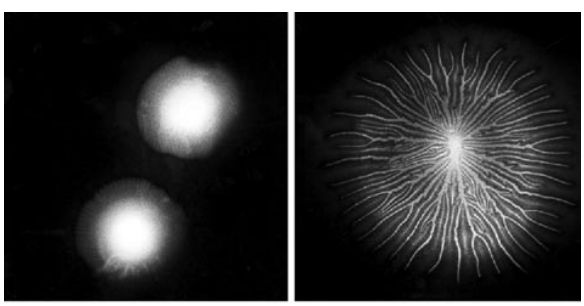

Figure 3. Discharge patterns (photographs in the visible spectrum range) on the dielectric surface (20 mm × 20 mm) of a VD arrangement: (a) bases of a VD on a dielectric anode (diffuse, homogeneous discharge distribution); and (b) the base of a VD on a dielectric cathode at a high rate of voltage increase (discharge channels on the surface).

2. Experimental findings

2.1. Discharge patterns

Depending on the gas mixture, pressure, discharge cell geometry and other parameters, a wide range of discharge forms were observed [15]. There were diffuse and continuously burning discharges as well as self-pulsing microdischarges of short duration, which are randomly distributed in time and space over the surface of the electrodes.

In VDs the charge transfer takes place within thin discharge channels, in microdischarges, which cross the discharge gap and are randomly distributed over the electrode surface at the conditions under consideration.

In figure 2 the streak photograph of a single microdischarge in air at atmospheric pressure is given [16]. There exists a cathode-directed streamer which seems to start in the middle of the gap and which then accelerates towards the cathode. As it reaches the cathode intensive processes happen in the whole discharge gap. After a few nanoseconds the intensity distribution is frozen and the discharge is extinguished comparatively slowly. The dark zone near the cathode may result from the high conductivity of the discharge column in this region. A detailed description

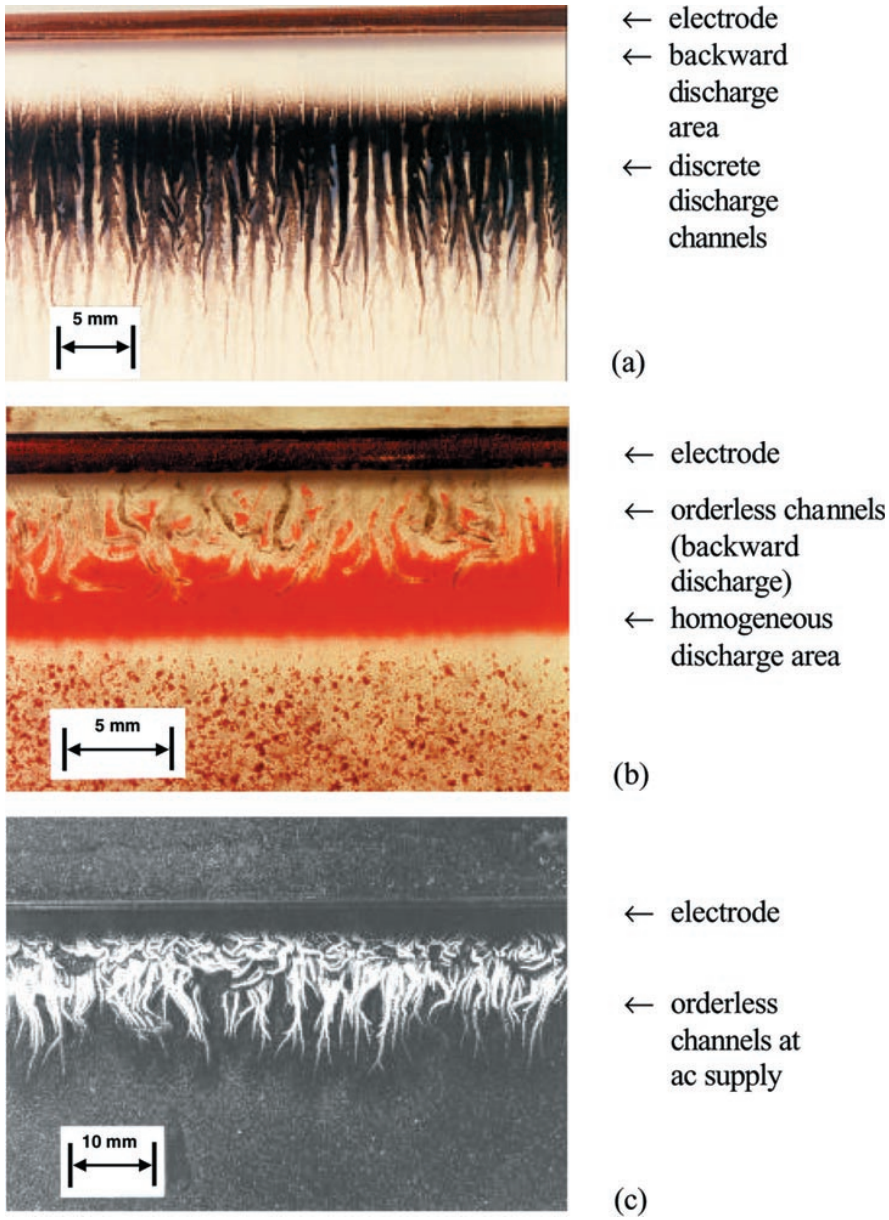

Figure 4. Discharge patterns on the dielectric surface of an SD arrangement (dust figures): (a) a positive voltage pulse of 20 kV at the surface electrode; (b) a negative voltage pulse of 20 kV; and (c) an ac voltage of 10 kV.

of the temporal behaviour of the microdischarge is given in [5]. The light intensity on the surface of the dielectric belongs to a surface discharge.

The bases of these channels on the surface of the dielectric ('surface discharges') depend on the polarity of the applied voltage (figure 3). When the dielectric is the cathode, distinct channels propagate from the discharge axis onto the dielectric surface (figure 3(b)). With the opposite polarity, a homogeneous and diffuse discharge area is observed (figure 3(a)).

The general character of the discharge patterns on the dielectric surface is independent of the arrangement (compare figure 3 with figure 4). In the SD case with positive polarity (a positive voltage at the surface electrode) distinct channels appear on the dielectric with widths in the order of magnitude of 1 mm (figure 4(a)). With the opposite polarity the discharge is uniformly distributed in a certain area along the electrode (figure 4(b)). As the voltage is decreased the potential difference between the surface charges and the electrode reaches breakdown field strength and 'backward' discharges with opposite polarity appear near the electrode. These back discharges have the patterns of the opposite polarity: at positive polarity they look uniform (figure 4(a)) while at negative polarity they consist of orderless channels (figure 4(b)). With an ac voltage a mixture of both patterns can be observed (figure 4(c)).

However, there is a distinct difference between the discharge mechanisms in the VD and SD arrangements. In VD arrangements microdischarge channels bridge the gas gap. The charge is transferred through these channels. With increasing voltage the number of microdischarges per period increases. In SD arrangements, however, there is no

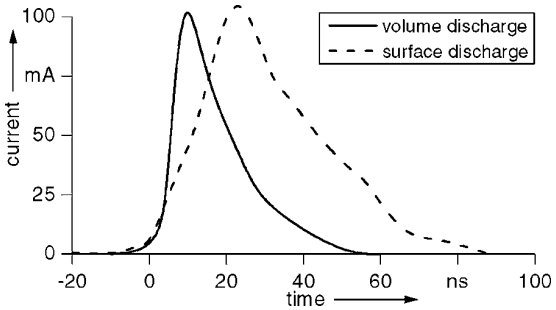

Figure 5. Typical shapes of measured current pulses in air at atmospheric pressure (SD: current per cm of electrode length).

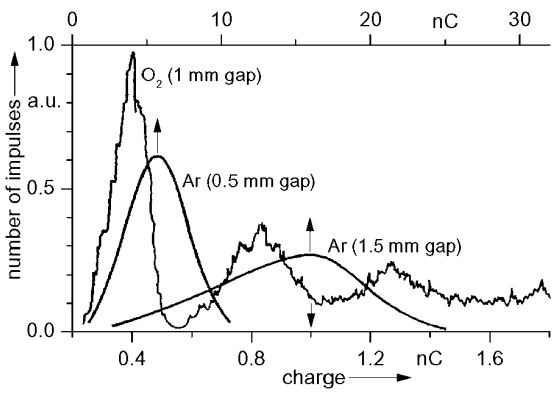

Figure 6. Distribution of the values of transferred charge in a small VD arrangement.

defined discharge gap. An increase in the voltage leads to an enlargement of the discharged area on the dielectric. In this case the charge transfer takes place in a thin layer on the dielectric surface.

2.2. Current pulses

Apart from the capacitance current, the current in DBDs consists of (numerous) short current pulses, which are a measure of the transferred charge. The current pulses are similar for both arrangements with the same boundary conditions. The time durations are comparable (figure 5) as well as the repetition frequencies, which depend on the shape of the voltage, the dimensions of the arrangement and the permittivity of the dielectric. The reduced rate of increase in current of the SD arrangement in figure 5 may follow from statistical effects, as the measurement was performed with a surface electrode 10 cm long.

In general, the shape and amplitude of the current pulse of a single microdischarge in VD arrangements are independent of the power supply as long as the rate of increase in the voltage is not too high (less than about 0.5 kV ns^{-1}). From this it follows that the charge transferred in a microdischarge is constant and that the total charge transferred during a half-period of voltage will only grow in discrete steps with increasing voltage. This has been found for electronegative gases like air or oxygen. It is not true for electropositive gases like argon, where a broad and continuous charge distribution exists (figure 6, [17]).

Free electrons initiate the breakdown process. The density (or number) of initial electrons may vary over a wide

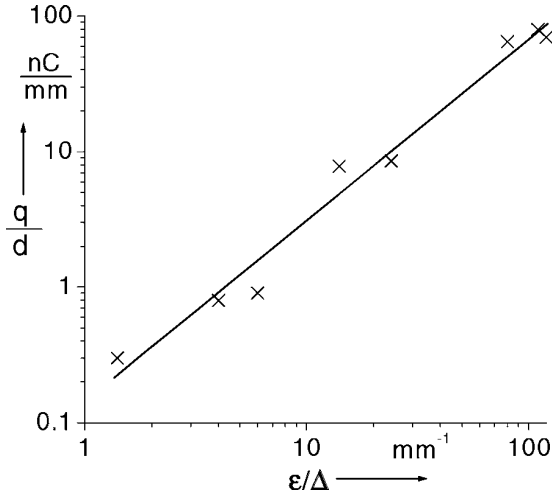

Figure 7. Related transferred charge q/d of microdischarges in VD arrangements depending on the specific capacitance ε/Δ of the dielectric (oxygen; d, Δ, discharge gap and thickness of the dielectric, respectively; ε relative permittivity).

range. As the charge transfer in electronegative gases can be easily reproduced according to figure 6, some mechanisms which uncouple the initial breakdown phase from the further development of the discharge must exist. The initial electrons play a trigger role only.

The actual quality of charge transferred through the discharge gap depends (apart from gas type and pressure) on the design parameters of the discharge arrangement, e.g. on the width of the discharge gap and the specific capacitance of the dielectric layer (figure 7). The electrode material has been found to have no effect on this value.

In SD arrangements the charges are distributed on the dielectric surface (figure 8). The length of the charged area perpendicular to the electrode depends on the polarity and amplitude of the applied voltage. For a single voltage pulse after discharge ignition, the SD grows stepwise as the voltage rises to its maximum (figure 9). During a voltage decrease, the potential difference between surface charges and the electrode causes backward discharges (figures 4(a) and (b)). Backward discharges reduce the charge density near the surface electrode; however, they do not influence its value a long distance from the electrode (figure 8(b)).

The measured charge density distributions in figure 8 correspond to mean values obtained from an electrode 6 cm in length. In fact, the charge distribution on the dielectric surface is not homogeneous. The positive charge density is presented in figure 8 because the discharge area is larger for this polarity and can be measured more precisely.

From the measurements it follows that, with negative polarity, successive discharge steps enlarge the size of the uniformly discharged layer on the surface with an increasing voltage only. With positive polarity the discharge step consists of a set of channels (figure 4). The positive polarity channels leave strips of charges on the dielectric surface. As voltage is increased, breakdown conditions are restored near the tips of the charge strips and the channels grow stepwise. The stepwise growth of the channels is accompanied by short current impulses in the external circuit (figure 9).

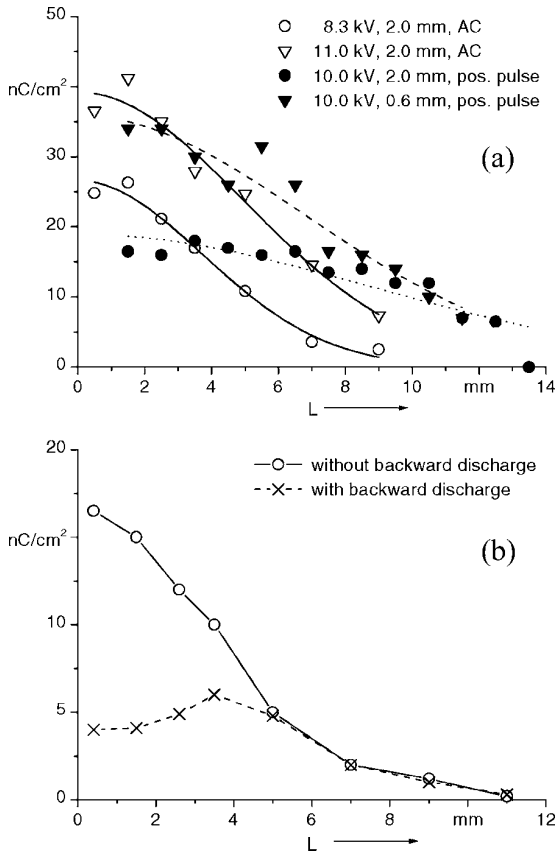

Figure 8. Measured charge density distribution on the dielectric surface of an SD arrangement in air at atmospheric pressure: (a) at different ac voltage amplitudes and single positive voltage pulses, respectively, and with different thickness of the dielectric; and (b) charge density before and after the backward discharge took place, ac voltage.

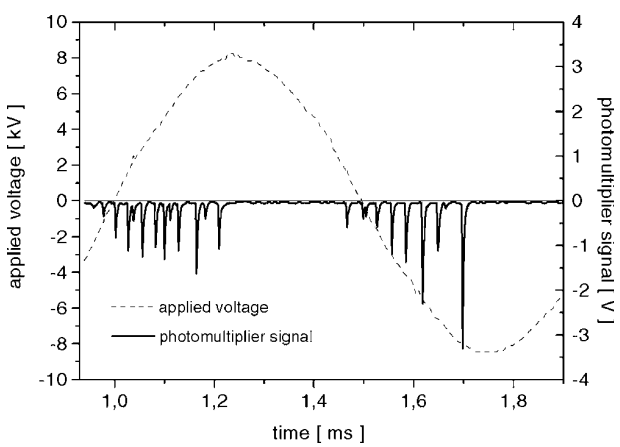

Figure 9. Photomultiplier signal of the radiation of an SD (in the visible spectrum range) during a period of applied voltage (representing current flow in the discharge).

The charged area on the dielectric surface is extended by approximately several millimetres with negative polarity. With positive polarity the channel extension is considerably larger (figure 10). With an ac voltage the discharge extension is between that with positive and negative polarity (figure 10). The outer boundary of the charged area is determined

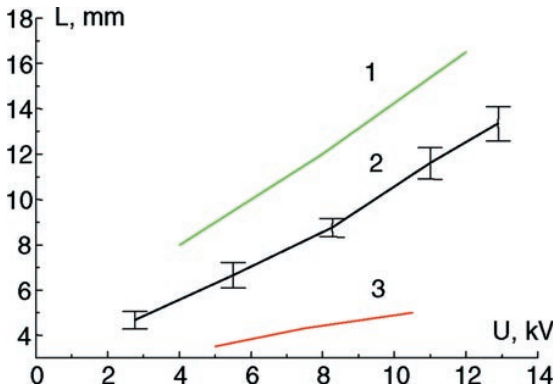

Figure 10. Lengths of discharge channels with (1) positive and (3) negative voltage pulses on uncharged surfaces and (2) those for ac voltage (peak values) with identical boundary conditions.

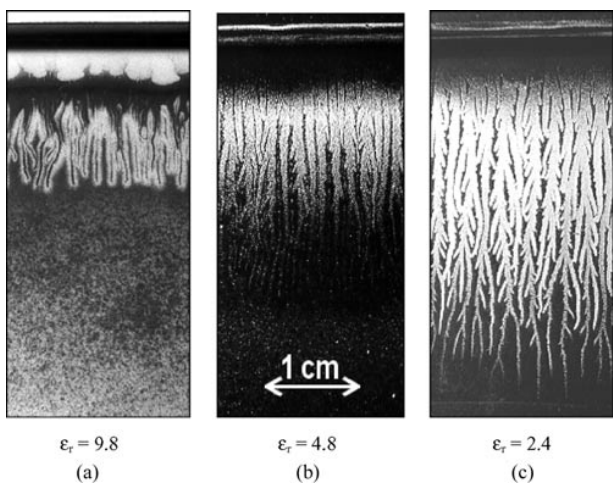

Figure 11. Dust figures of surface discharges on dielectrics with different relative permittivities and otherwise identical conditions: (a) Al_2O_3, (b) borosilica glass, (c) PETG.

by the first positive half-cycle of the applied voltage. In the succeeding negative half-period the negative charged layer is extended by the outer positive charges on the surface, enhancing the field strength component parallel to the surface. It has been proved experimentally that with an ac voltage the outer region of the surface charge layer is charged positively [8].

With constant level of applied voltage the length of the discharge patterns depends on the relative permittivity value of the dielectric (figure 11). The larger the permittivity is the shorter the discharge length becomes.

As already mentioned, the size (or length) of the charged area in SD arrangements also depends on the amplitude of the voltage. From this, it follows that the dielectric area involved in the discharge process is not constant or, in other words, the capacitance of the discharged area depends on the voltage amplitude. This is quite different to VD arrangements and results in different current–voltage characteristics (figure 12). The characteristics reflect the formal dependence between the applied voltage and average current through the discharge arrangement as an element of the external circuit. It is interesting to note that the characteristics practically do not depend, for example, on the type of gas but mainly on the capacitance of the arrangement.

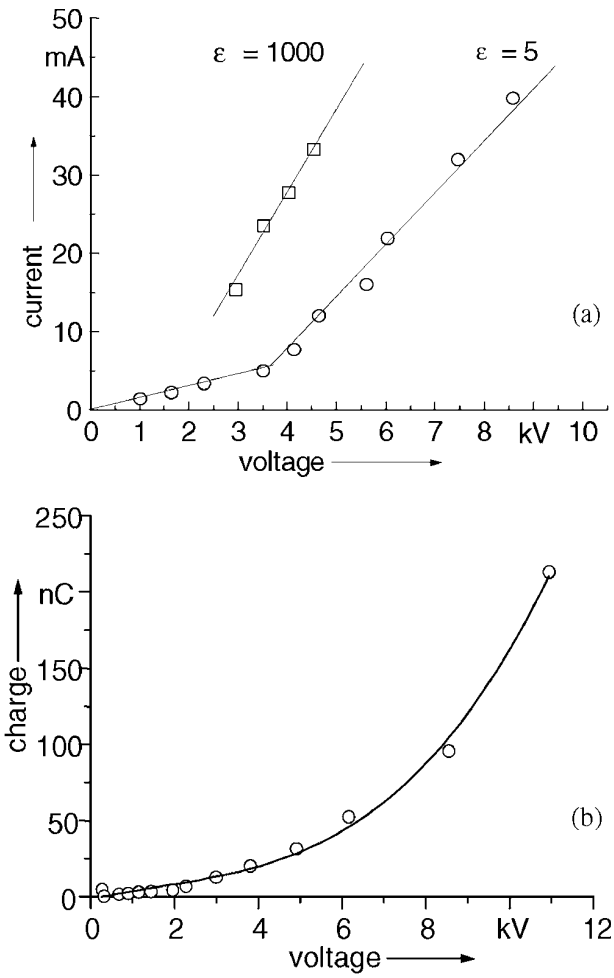

Figure 12. Current–voltage characteristics of (a) a VD arrangement (discharge gap 1 mm, 150 Hz, air at atmospheric pressure) and (b) an SD arrangement (relative permittivity 5, thickness of dielectric 2 mm, frequency 2 kHz, length of surface electrode 12 cm, oxygen at atmospheric pressure).

The current up to the bend in the curve ($\varepsilon_r = 5$, glass) in figure 12(a) is a displacement current. Prolonging the characteristic to the x-axis one can obtain the lowest possible burning voltage for the discharge gap. This value is about 2.8 kV for $\varepsilon_r = 5$ and 1.4 kV for $\varepsilon_r = 1000$ (ceramics, based on TiO_2). These are effective values; the amplitude will be about 2.0 kV for $\varepsilon_r = 1000$. It is at least 1.5 times lower than the breakdown voltage of a 1.0 mm gas gap in oxygen at atmospheric pressure, which can be found from the Paschen curve. The difference can be explained by the influence of charge carriers accumulating on the dielectric surface. It is less pronounced for dielectrics with the permittivity of glass; however, for a relative permittivity of 1000 this influence becomes more important and the burning voltage drops significantly below the ignition voltage. This phenomenon is widely exploited in plasma display panels by using the differences in the ignition and operating voltage.

3. Dynamics of charged particles

3.1. Equations and boundary conditions

Numerical modelling is useful in understanding the dynamics of the DBD development in more detail. In general, a three-dimensional description is necessary. However, as axial symmetry exists in VD arrangements and as in SD negative polarity configurations the discharge is uniform along the electrode, two-dimensional modelling is a good approach. With positive polarity SDs (figure 4(a)) the inter-channel distance is much narrower than the channel length so a two-dimensional description is also reasonable.

Using the local field approximation, the temporal and spatial development of the particle densities (of electrons, ions and other components of the discharge) can be described by the following system of continuous equations:

$$\frac{\partial n_i}{\partial t} + \operatorname{div}(n_i + \boldsymbol{v}_i) + \operatorname{div}(D_i \operatorname{grad} n_i) = S_i \qquad (1)$$

where n_i, $\boldsymbol{vi}$, D_i and S_i are the particle density, drift velocity, diffusion coefficient and the source term of the ith component, respectively.

The initial densities of the components in the discharge region are

$$n_i(\boldsymbol{R}, t = 0) = n_i^0(\boldsymbol{r}) \qquad (2a)$$

where $\boldsymbol{r}$ is the vector of the co-ordinates.

The dielectric surface is defined as an impermeable boundary. All charged particles reaching this boundary are collected on the surface. Electron emission at the cathode by photons and positive ions were taken into account by

$$n_e v_e = \gamma_+ n_+ v_+ + \gamma_{ph}\phi \qquad (2b)$$

where γ_+ is the second Townsend ionization coefficient for ions and γ_{ph} that for photons. ϕ is the photon flux density on the surface. As the photon emission at any point $\boldsymbol{x}_i$ is considered to be proportional to the ionization rate at point $\boldsymbol{X}_j$, ϕ is obtained by integrating the ionization rate over the whole volume of the discharge region:

$$\phi = B \int \frac{\alpha n_e v_e}{|\boldsymbol{X}_j - \boldsymbol{x}_i|} \cos(\boldsymbol{X}_j \boldsymbol{x}_i)\, \mathrm{d}V \qquad (3)$$

where B is a constant and $\cos(\boldsymbol{X}_j \boldsymbol{x}_i)$ defines the angle of incidence of photons reaching the dielectric surface.

In order to get the actual field configuration equation (1) must be completed by the Poisson equation:

$$\Delta\varphi = -\frac{1}{\varepsilon_0}\rho(\boldsymbol{r}, t) \qquad \text{(in the gas gap)}$$

$$\Delta\varphi = 0 \qquad \text{(in the dielectric)} \qquad (4)$$

where $\rho(\boldsymbol{r}, t)$ is the space-charge density at position $\boldsymbol{r}$. At the boundary between the gas (g) and the dielectric (d) the following relations for the tangential (E_t) and normal (E_n) component of the electric field strength are valid:

$$E_{gt} = E_{dt}$$

$$E_{gn} = \varepsilon E_{dn} + \frac{1}{\varepsilon_0}\sigma(\boldsymbol{r}, t) \qquad (5)$$

where $\sigma(\boldsymbol{r}, t)$ is the surface charge density.

To solve equations (4), the boundary conditions must be known. For VD arrangements the potential or field strength conditions at the boundaries can be defined *a priori*. For SD arrangements this is impossible. The potential along the boundaries of the integration region is unknown. To find the values an image charge method was used.

3.2. Modelling procedure

The potential distribution at the boundaries of the integration region is determined from the surface charges on the conductive electrodes, the surface charges on the dielectric and the charge density in the discharge region. The charge-density distribution in the discharge region as well as the surface charge can be found by solving the continuity equations (1). The charges on the conductive electrodes are unknown.

The conductive electrode surface is an equipotential area. The potential is found by the superposition of all charges involved. Thus, the charges in the discharge region, on the dielectric surface at the electrodes, together with their image charges, give a linear equation, which links their values with the potential at a certain point,

$$\boldsymbol{A} \cdot \sigma + \boldsymbol{A}^{v} \cdot \boldsymbol{q} = \boldsymbol{V} \tag{6}$$

where $\boldsymbol{A}$ is the distance matrix between the volume as well as the surface charges (σ) and the control point on the conductive electrode; $\boldsymbol{A}^{v}$ is the distance matrix between charges on the electrode ($\boldsymbol{q}$) and the control point on the conductive electrode; $\boldsymbol{V}$ is the known potential of the conductive electrode.

Solving equation (6), the unknown charges $\boldsymbol{q}$ on the conductive electrodes are determined and the potential at the boundary of the integration region, i.e. the Poisson equation (4), can be solved.

The numerical procedure is described in [14]. The time scale is divided into time steps. At each step, the set of continuity equations is solved. In order to eliminate numerical diffusion a flux correction transport (FCT) routine was used [14].

The swarm parameters as well as the rate constants for the elementary processes are assumed to be proportional to the local field strength (local field equilibrium approximation).

The drift velocities and swarm parameters are taken as functions of the reduced field strength [18, 19].

3.3. Initial phase of the discharge

In order to ignite a discharge initial electrons are needed. They may emerge from natural ionization sources and/or residual charges from previous discharges. Initially the total number of electrons is small, but as the electrons move from the cathode to the anode the number of electrons multiplies to such an amount of charge which can be measured. In VD arrangements the field distortion becomes significant at an electron density of about 10^{12-13} cm^{-3} (at atmospheric pressure) [14].

When the first avalanche reaches the anode there is no significant amount of free electrons within the gas gap. The only electrons that can exist at this time result from detachment or emission processes on the cathode. The total current and transferred charge caused by the initial electrons and the first avalanche are negligible and far from values that could be measured. That is why there must be a mechanism which is triggered by the first avalanche and which transforms the potential energy of the electric field into further development of the discharge process and hence increasing the current.

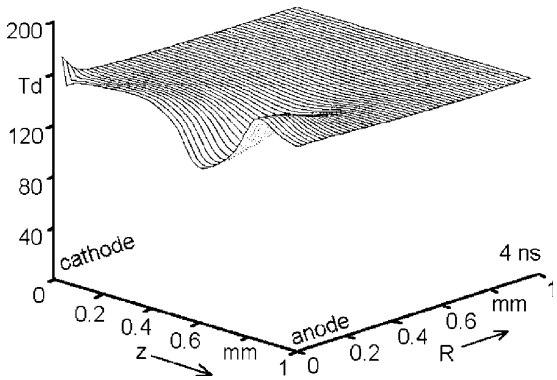

Figure 13. Field strength distribution in the discharge gap during the initial phase of a VD (in air at atmospheric pressure).

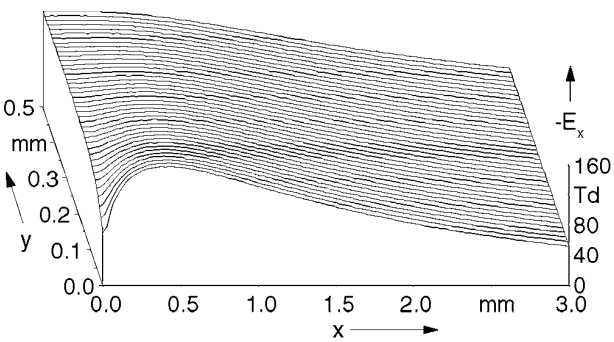

Figure 14. Initial distribution of the tangential component of the electric field strength (parallel to the dielectric surface) of an SD arrangement (wire electrode with a flat base on a dielectric plate, figure 1).

The first avalanche disturbs the field distribution only slightly (figure 13). The multiplication coefficient of the electrons is still at its initial level. Secondary electrons from the avalanche photons continue to generate additional photons which, in turn, create further photoelectrons at the cathode. This is a self-reinforcing process. Passing through the region of field distortion, secondary electron clouds continue to enlarge the field distortion and shift it towards the cathode. After some time the electric field distortion becomes high enough to initiate a cathode-directed streamer [14].

In SD arrangements (diameter of the surface electrode about 1–3 mm and a relative permittivity of the dielectric layer of up to 50) such a reinforcing effect does not appear. The initial field strength distribution is non-homogeneous (figure 14) and the extension of the discharge on the dielectric surface is, in general, several times larger than the gap distance in the typical VD arrangement under consideration. This is why cathode-directed streamers have not been observed when modelling SD development. However, secondary processes on the cathode surface do take place. In principle, it should be possible to find the conditions under which the discharge process in SD arrangements will become intensive enough to cause streamer transitions.

In the SD case the initial phase of the discharge differs from that in VD arrangements. Because of the initial non-homogeneous electric field distribution there is only a

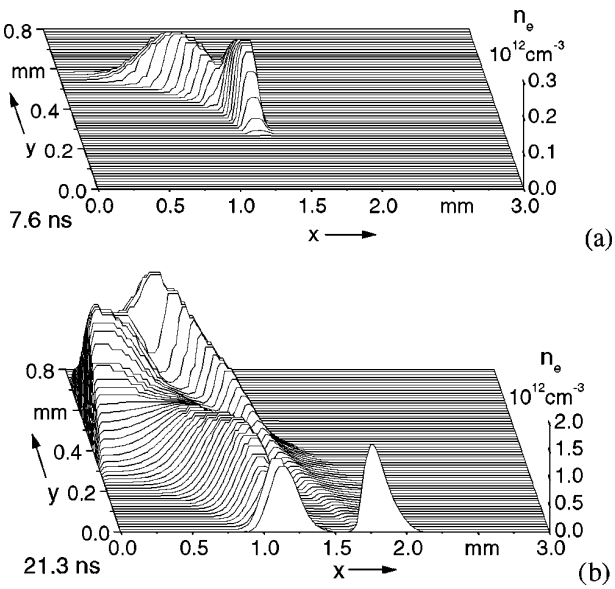

Figure 15. Development of the electron density in air at atmospheric pressure of an SD arrangement with a wire electrode of 1 mm radius and an initial voltage of -11 kV at two time steps ($\varepsilon_r = 8$, thickness of the dielectric 2 mm, air at atmospheric pressure).

short region where the effective multiplication coefficient of electrons is positive. Initial electrons multiply in number and move away from their initial position near the surface of the cathode towards the dielectric surface (figure 15(a)). Reaching the region with a negative effective ionization coefficient the total number of electrons in the first avalanche decreases; electron attachment processes exceed those of electron multiplication.

From the very beginning the initial cloud of electrons permanently generates secondary electrons via photoemission, which causes the tail behind the first peak in the electron density distribution of figure 15(a). In this phase of the discharge electrons move to the dielectric surface continuously, irradiating the cathode and causing secondary electrons permanently.

As the initial phase develops, the first avalanche reaches the surface (at 1.8 mm in figure 15(b)). Photoemission from the tail of this avalanche causes a significant flux of electrons between the position of the first avalanche and the dielectric surface (figure 15(b)). A second surface charge maximum appears in the charge distribution on the surface, which belongs to secondary avalanches. Later on these maxima grow together (figure 16(a)) and the surface charge density reaches a saturation level. A further accumulation of charges on the surface is only possible at larger distances from the cathode, i.e. electrons move in a thin layer above the surface and are deposited on the surface at the far end of the surface charge distribution (figures 16(a) and (b)). This movement along the dielectric surface resembles an ionization wave.

The electron movement is connected with a modification of the electric field. The normal component of the electric field strength in front of the charged area on the surface becomes zero (figure 17(a) between 1 and 2 mm), so that there are no forces directed to the surface and the electrons move along the charged surface. The position of the electron

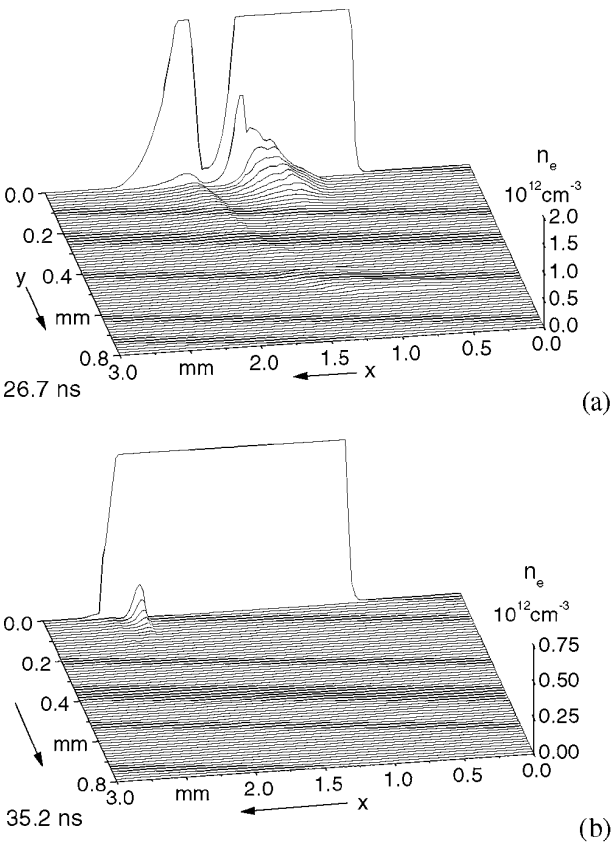

Figure 16. Electron density distribution of an SD at two time steps (conditions as in figure 15).

density distortion (figure 16(b) at 35.2 ns) is connected with the maximum of the tangential component (parallel to the surface and perpendicular to the electrode) of the electric field strength (figure 17(b)).

The charge transfer in both VD and SD configurations starts with the initial electrons. The movement of the first avalanche through the discharge region and the growth in the number of electrons result in a change in the initial distribution of the electric field strength. The field increases near the charge density maximum. Secondary electrons passing this field distortion are responsible for an increase and further development of the photoemission processes at the cathode.

This self-reinforcing effect changes the dynamics of the initial phase of the barrier discharges, from the kinetics of the first avalanche to the dynamics of the secondary electron current. Differences in the development of the discharge in both configurations appear later on.

3.4. Streamer formation and propagation

The continuous current flow during the initial phase of the discharge causes a certain charge accumulation in the discharge region. This accumulation changes the field strength distribution and finally causes an ionization wave in both arrangements.

In SD arrangements with dimensions which are typical for ozone generators this wave propagates towards the anode along the dielectric surface (figure 15–17). However, the

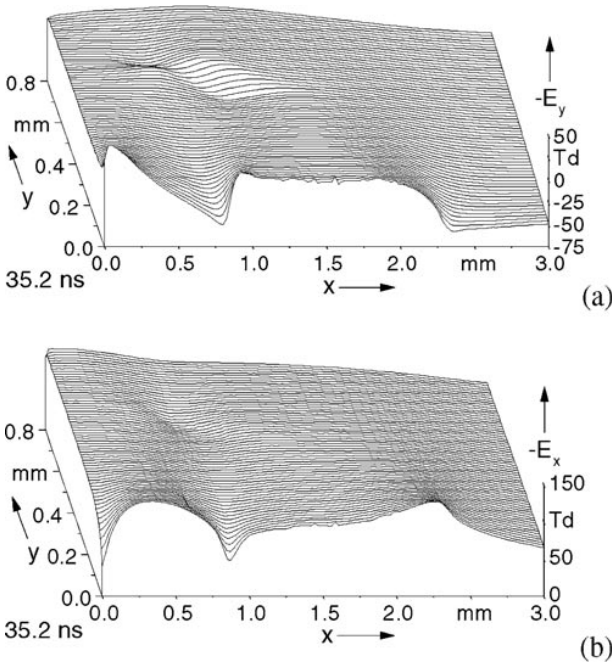

Figure 17. Normal (a) and tangential (b) components of the electric field strength during the propagation of an ionization wave (conditions as in figure 15).

generation of secondary electrons at the cathode is not strong enough to create a well-developed streamer. The propagation of the anode-directed ionization wave in SD arrangements stops after a distance of a few millimetres because of the decreasing field strength distribution and can only be continued after a considerable increase in the applied voltage.

The VD case is characterized by short discharge gaps (of the order of 1 mm). Because of this and the initial uniform field strength distribution in the gap, secondary electrons are generated faster with a stronger reinforcing process in comparison with SD arrangements leading to a cathode-directed streamer (figure 2). These features are evident in figure 18 where a simulated streak photograph of a microdischarge in air at atmospheric pressure is presented. Initial electrons generate an avalanche near the cathode. At about 3 ns the electron density in the avalanche becomes high enough, on one hand, to distort the initial electric field distribution and, on the other hand, to be detected in the simulation (the darkness is proportional to the rate of ionization). Between 5.5 and 7 ns there is no radiation to be seen. This follows from a reduction of the sensitivity of the simulated streak photograph at this time and from the behaviour of secondary electron clouds which reach the anode and are collected on the dielectric surface.

After about 7 ns secondary electrons are passing the electric field distortion (at about $z = 0.8$ mm) resulting in a strong radiation because of the high value of the ionization coefficient at this position. At this moment the positive-ion density near the cathode is low.

The secondary electrons result mainly from photoemission processes at the cathode; ion impact emission is of less importance. The field strength distortion results in the appearance of a cathode-directed streamer. The time interval

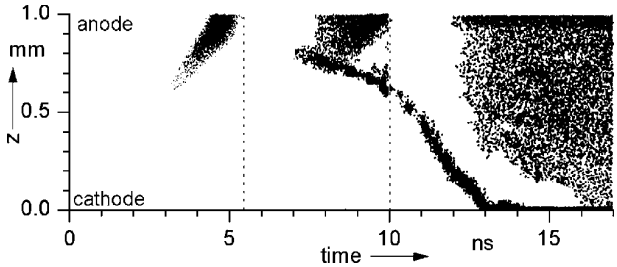

Figure 18. Streak photograph of the VD channel development in air at atmospheric pressure (modelling results, at the dotted lines the sensitivity changes; dielectric anode, $\varepsilon_r = 5$, thickness of the dielectric 2 mm, air at atmospheric pressure).

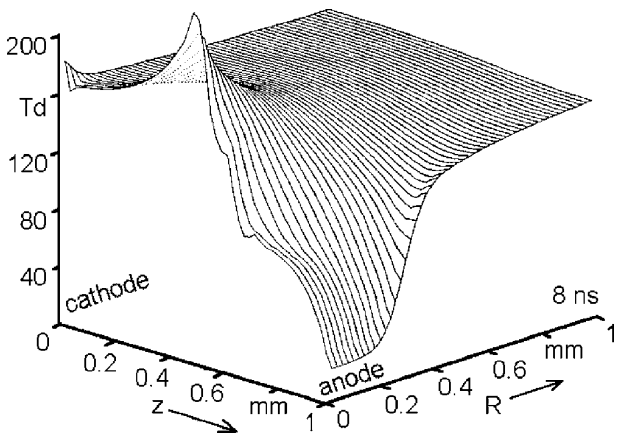

Figure 19. Axial component of the electric field strength of a VD during the streamer phase at 10 ns (compare figure 18).

from when the discharge process first begins to the moment when the streamer appears requires about twice the time of flight of electrons travelling from the cathode to the anode.

As the streamer starts to propagate (at 7 ns) its velocity is slightly less than the electron drift velocity. The streamer accelerates later on (at about 10 ns) and its velocity increases considerably. The maximum value of the field distortion is near the head of the streamer (figure 19). The amplitude of this distortion is nearly twice the initial value. At this moment the streamer velocity may exceed the drift velocity of the electrons in the undisturbed field. The time interval between the appearance of the streamer and the further acceleration of its propagation is about the drift time of electrons from the cathode to the streamer head (3 ns). A wave of secondary electrons resulting from photoemission processes meets the streamer at a distance of 0.6–0.7 mm from the cathode and causes an increase in the streamer propagation velocity (figure 18).

Behind the streamer head a well-ionized channel with high densities of charged particles and corresponding low field strength appears. The value of the field strength in the channel is about half of the initial one (figure 19, compare the field strength values between 0–0.4 mm with that between 0.7–1.0 mm). At this level of field strength the effective value of the first Townsend ionization coefficient is about zero. The movement and multiplication of electrons is determined by a self-sustaining equilibrium. A decrease in the mean electric field strength within the conductive channel, for example, increases the attachment processes and the electron density

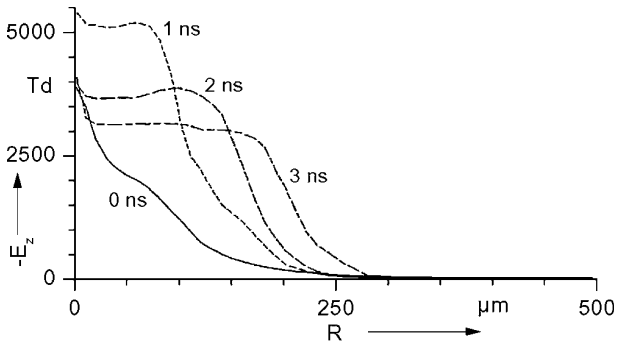

Figure 20. Radial distribution of the axial field strength component at the cathode of a VD arrangement (at $t = 0$ the streamer has reached the cathode).

decreases. A reduction in the electron density, however, causes field strength increase up to the equilibrium value and vice versa.

The propagation of the streamer head causes a growth in the length of the well conducting channel. This compresses the potential between the head of the cathode-directed streamer and the cathode surface with a rapid rise in the field strength. It reaches a value of a few thousand Townsend at the cathode. At this moment (13 ns in figure 18) a conduction channel connects the electrodes.

3.5. Cathode layer formation and discharge extinction

The cathode layer in VD arrangements develops from the moment when the streamer reaches the surface of the cathode (13 ns in figure 18). The field strength in the double layer of electrons and positive ions near the cathode reaches values more than 30 times higher than the initial value in less than a nanosecond (figures 18 and 20). From this moment photoemission at the cathode is widely substituted by electron emission via positive ions, i.e. photoemission becomes negligible. If we omit photoemission in the simulation process the duration of the initial phase increases by about an order of magnitude. The double-layer formation is connected with a radial propagation of the cathode layer (figures 20 and 21). This propagation results from the radial field strength distribution. The value of the radial component is comparable to the value of the initial field strength (figure 21(a)). During the radial propagation it decreases (figure 21(b)) and vanishes finally. The impedance of the circuit, especially the specific capacitance of the dielectric, determines the enlargement and final extension of the cathode layer.

In SD arrangements the situation is quite different. The current density estimated from measurements is an order of magnitude lower than that in VD arrangements with comparable conditions. The low current density is not compatible with a cathode layer in general. In other conditions, however, e.g. with enlarged secondary electron emission, something like a cathode layer may appear.

In VD arrangements the accumulation of surface charges on the dielectric is the starting point of the extinction process of the discharge. The surface charges build up a counter field so that the effective field strength in the gap decreases and the discharge process diminishes.

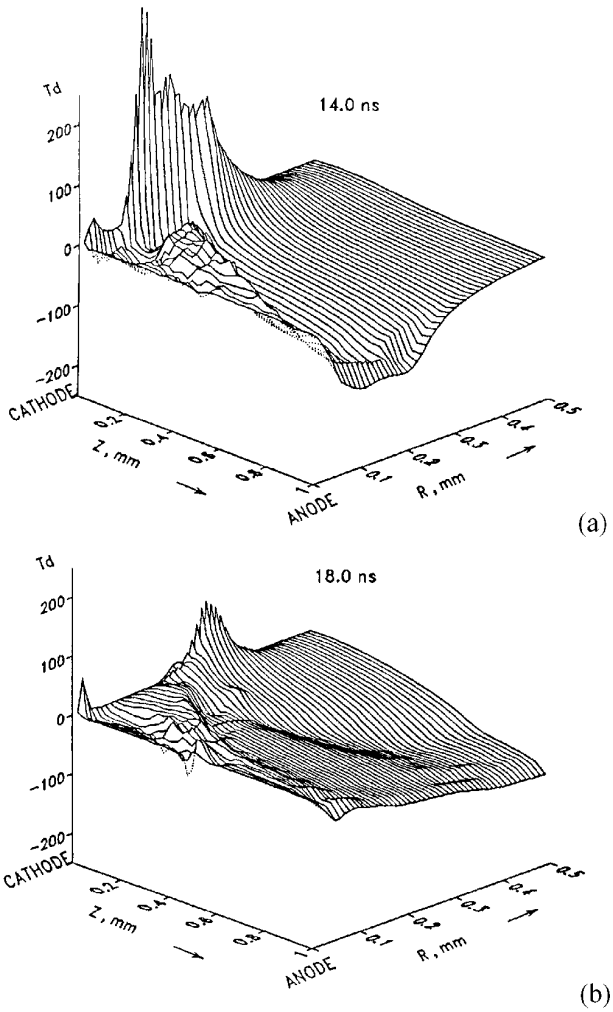

Figure 21. Distribution of the radial component of the electric field strength in the cathode layer and the conductive channel in a VD arrangement at the beginning of the radial propagation of the cathode layer (a) and later on (b).

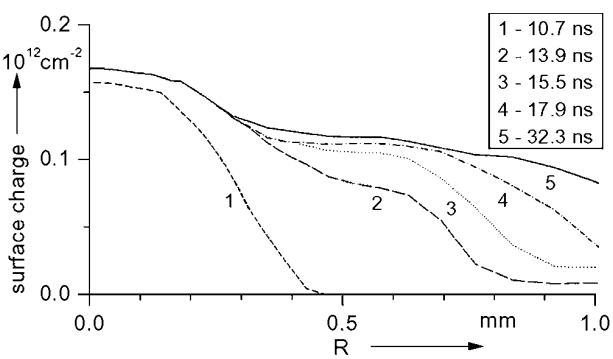

Figure 22. Distribution of the surface charge density (in electrons per cm^2) on the dielectric surface (anode) of a VD arrangement (relative dielectric constant 5, discharge gap 1 mm, pressure 1 bar air).

The maximum of the surface charge density appears on the channel axis (figure 22). Although the surface starts charging with the first avalanche, a considerable charge accumulation begins during streamer propagation. From figures 18 and 22 it follows that a significant surface charge

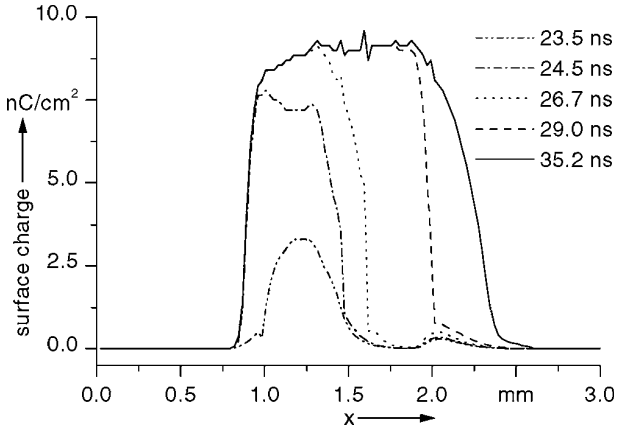

Figure 23. Distribution of the surface charge density of an SD pulse (air, thickness of the dielectric layer 2 mm, relative dielectric constant 5, other conditions as in figure 15).

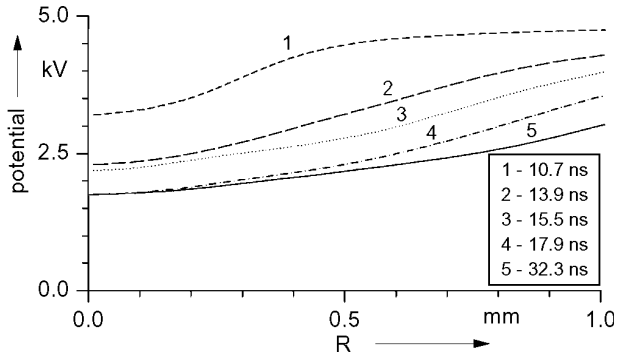

Figure 24. Potential distribution on the dielectric surface (anode) of a VD arrangement (conditions as in figure 22).

density appears during the acceleration of the streamer propagation. Its maximum is a saturation value, which never will be exceeded during the charge accumulation process because of the radial movement of charge carriers ('surface discharge'). It is defined by the specific capacitance of the dielectric at the given conditions and is in the order of 10–30 nC cm^{-2} for both the SD and VD arrangements with comparable specific capacities and the typical conditions under consideration (figures 22 and 23).

The distribution of the radial field strength component in VD arrangements is correlated to the distribution of the accumulated charge at the anode (compare figure 21 with figure 22). This component grows from zero on the axis (at the anode side) to a distance of about 0.2 mm from the axis at $t = 14$ ns in figure 21(a). As the normal component of the electric field strength near the surface charge is zero, electrons move along the surface charge enlarging the size of the charged surface and, hence, the size of the area where the potential in the discharge channel decreases. Finally, the potential drops to about 60% of its initial value and the radius reaches 1.0 mm (figure 24). This is several times larger than the channel radius.

The saturation values of the surface charge density have been found for both arrangements and are comparable. In the SD case it is about 10 nC cm^{-2} in figure 23. The absence of surface charges in the region near the cathode up to about 0.8 mm in figure 23 can be explained by the special form of the electrode in the simulation. Because part of the cathode surface is perpendicular to that of the dielectric, the normal component of the electric field strength is about zero in the region near the electrode and the charge accumulation starts at a certain distance from the cathode.

The dynamics of charge accumulation in both arrangements (SD and VD) are, in general, the same. Differences result from the differing processes at the surface. In SD arrangements the interaction of the initial non-homogeneous field configuration with the charges accumulated on the surface results in an ionization wave, which moves along the surface (figures 15 and 16). The further accumulation of charges on the dielectric surface leads to a decay in the charge transfer and later on to an extinction of the discharge (step) as a whole.

In the VD case the shielding effect of adsorbed charges freezes the radial propagation of the cathode layer at first and then decreases its current density. Simultaneously the value of the current reaches its maximum value and then declines. This process can be illustrated qualitatively by the values of the current density in the cathode layer. At the very beginning of the radial propagation of the cathode layer it is about 200 A cm^{-2}, at current maximum 60–65 A cm^{-2}, only (table 1).

The influence of the external impedance on the parameters of the cathode layer is clear from the data in table 1 as well. The well known fact that the decrease of the buffer resistance increases the diameter of the cathode layer [20] has been confirmed by modelling. The area of the cathode layer is proportional to the dielectric constant. The amplitude of the current also rises with permittivity. The calculated parameters of the cathode layer in table 1 are in satisfactory agreement with those of normal glow discharges found in the literature [20].

In figure 25 distributions of the electric field strength, densities of electrons and positive ions are presented within a layer of 100 μm at the cathode of a VD arrangement. The double layer of electrons and ions can clearly be distinguished. The thickness of the positive-ion layer at the cathode is about 20 μm (figure 25(c)). The maximum of the electron density is situated 20 μm away from the cathode (figure 25(b)). Within the positive-ion layer the axial electric field strength increases from 3000 to 4000 Td (figure 25(a)). Outside the cathode layer in the conduction channel the total charge density is about zero. This means the channel is quasi-neutral. The radial size of the cathode layer in figure 25 as well as that of the conductive column is about 600 μm. A decrease in the charge densities towards the discharge axis can be detected in figure 25(b).

The decrease results from the shielding effect of adsorbed charges on the dielectric, which starts at the centreline of the discharge and initiates the extinction process.

After cathode-layer formation all parameters in the cathode layer and discharge channel stabilize. Any further change happens comparably slowly. The field strength in the conductive channel is practically constant over the channel length (figure 26(a)). Its level is frozen at a value of about 90–100 Td, which is not far from the level where the effective ionization coefficient is zero. That is why electrons move through the channel without any significant multiplication.

Table 1. Parameters of cathode layers in VD arrangements at current maximum (conditions as in figure 18).

Relative permittivity	Current amplitude (mA)	Radius of cathode layer (μm)	Current density (A cm^{-2})	Cathode fall (V)	Thickness of cathode layer (μm)
5	100	200	65	450	20
50	600	600	60	650	16

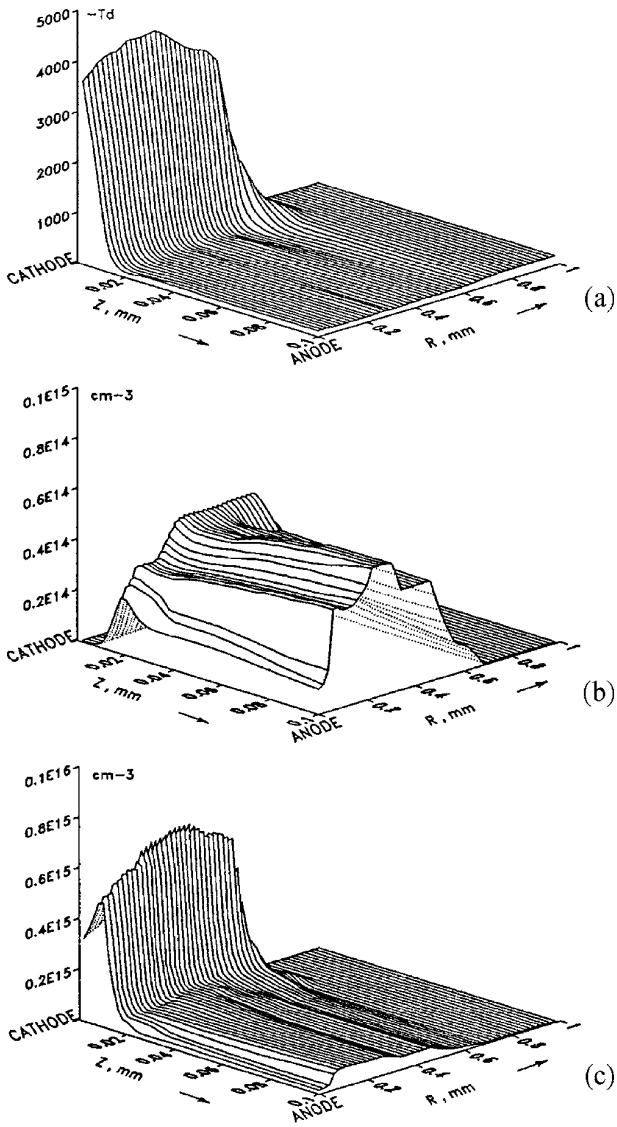

Figure 25. Distributions of (a) axial electric field strength, (b) the densities of electrons and (c) positive ions at current maximum in the neighbourhood of the cathode of a VD arrangement (conditions as in figure 22 except $\varepsilon_r = 50$).

The electron density along the discharge channel changes only slowly. Its maximum is in the middle of the gas gap at peak current. A reduction in the electron density on the discharge axis can also be detected. Its minimum is in a distance of about 0.4 mm in figure 26(b) and is the result of the shielding effect. First of all, the shielding influences the current density in the cathode layer. After that the electron density minimum moves from the cathode to the anode. Combined with this the anode potential decreases

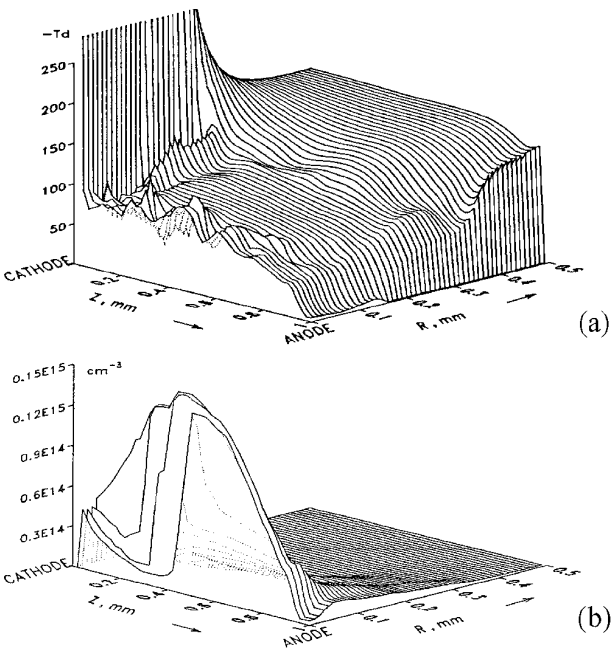

Figure 26. Distributions of (a) the electric field strength and (b) the electron density at the maximum current of a VD arrangement ($\varepsilon_r = 5$, oxygen 1 bar).

and propagates in a radial direction from the channel axis to the outer region (figure 24). Simultaneously the cathode current density decreases. The farther apart from the channel axis the later the density reduction appears (figure 26(b)).

The channel size can be determined from figure 26(a). Its radius is defined by the radial size of the cathode layer and is about 200 μm. Because of the accumulation of surface charges on the dielectric it increases at the anode.

4. Discharge development on pre-charged surfaces

4.1. Influence of pre-charged surfaces on the discharge development

Up to now the dynamics of DBDs on non-pre-charged surfaces has been considered. With an increasing ac voltage, however, discharge pulses spread over pre-charged surfaces. In other words, the initial conditions for successive discharge pulses are given by the charge distribution on the dielectric surface of the preceding discharge pulse.

At the end of the charge transport of a preceding discharge pulse, a layer of charges with a structure depending on polarity remains on the dielectric surface. In the VD arrangement, the discharge pulse consists of a set of microdischarge channels, which develop perpendicularly to the electrodes. The charge layer on the dielectric does not

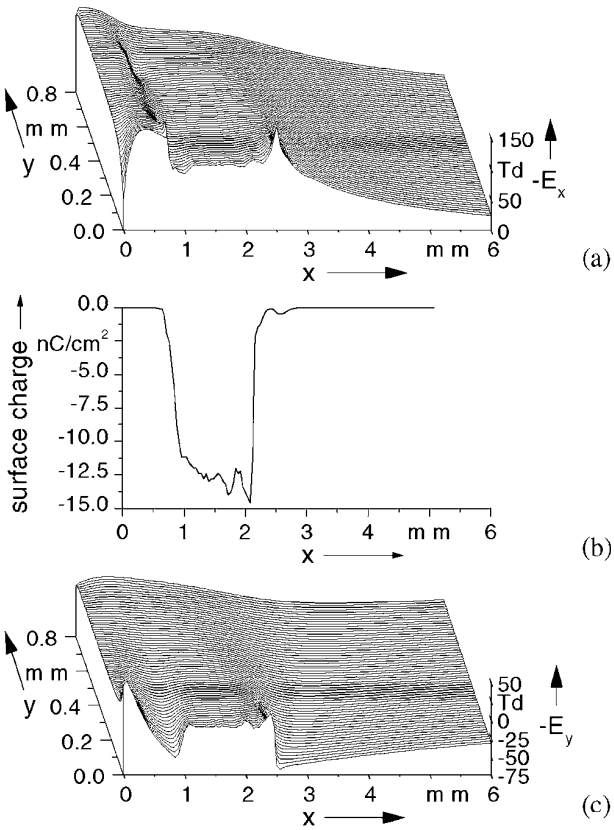

Figure 27. Initial distributions of (a) the tangential (parallel to the surface) and (c) normal component of the field strength with a negatively pre-charged surface and (b) corresponding surface charge density.

change the shape of the initial field strength distribution of succeeding microdischarges substantially. On increasing the voltage, successive microdischarges appear in between the bases of preceding ones. On changing the polarity of the applied voltage the local field strength is slightly higher at locations with surface charges on the dielectric than it is at adjacent locations. This determines the location of the following microdischarges on the dielectric; however, in general the initial conditions of the succeeding discharge channel are the same.

In SD arrangements, the situation is more complicated. Successive discharge steps develop on the dielectric surface at field strength distributions which are substantially influenced by the surface charges. The dynamics of future discharges changes because of differing initial field strength conditions. One can distinguish two cases. The first concerns the further enlargement of the external voltage up to its peak value, the second concerns the changes in polarity with a charged surface of opposite polarity.

If the dielectric surface is, for example, negatively charged and the external negative voltage is increased further, the normal component of the field strength above the charged area is nearly zero (figure 27). The tangential component (parallel to the surface) above the charged area has a plateau. This field configuration defines the trajectories of successive electrons. They move in a small gas layer above the dielectric surface up to the tip of the charged area and then turn to the dielectric surface (figure 28).

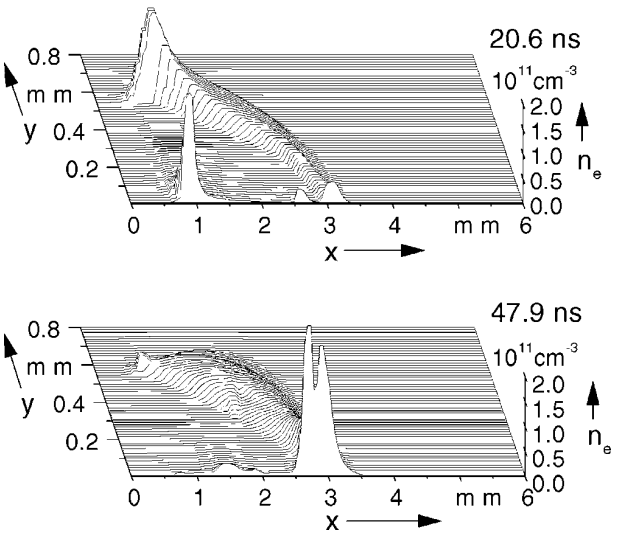

Figure 28. Development of the electron density on a negatively pre-charged surface and an initial voltage of −13.5 kV (see figure 27(b); radius of the wire electrode 1 mm, thickness of the dielectric 2 mm, $\varepsilon_r = 8$, atmospheric air pressure).

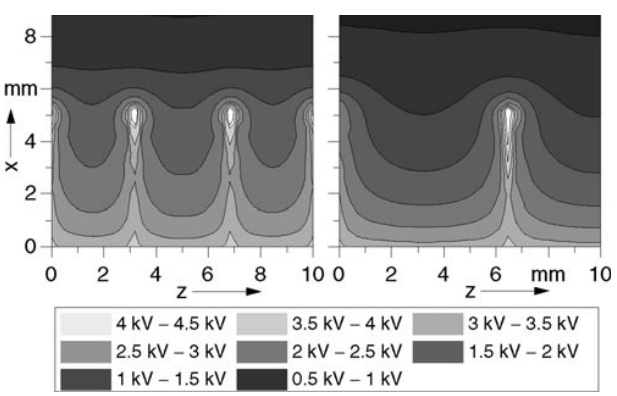

Figure 29. Simulated potential distribution of a surface discharge with positive polarity for different inter-channel distances ($\varepsilon_r = 5$, thickness of the dielectric 2 mm).

If the dielectric surface is positively charged and the external voltage changes sign, the initial conditions are quite different. The normal component of the field strength now has a certain value. It is about 100 Td at ignition conditions in air at atmospheric pressure, as has been found from simulations. This means the initial electrons will move directly to the centre of the surface charge, discharging the dielectric. During the discharge development, the surface charge also changes its sign.

These two cases, the discharge ignition at pre-charged surfaces of positive and negative polarity, comprise all possibilities for future discharge development. From measurements, it follows that, with negative polarity, successive discharge steps enlarge the size of the homogeneous discharge layer with increasing voltage, only. With positive polarity, the discharge step consists of a set of channels (figures 11 and 29).

The positive polarity channels leave strips of charges on the dielectric surface. With increasing voltage, breakdown conditions are restored near the tips of the charge strips and the channels grow stepwise. The stepwise growth of the

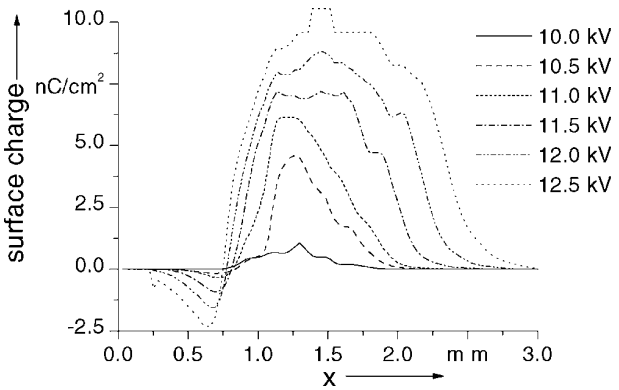

Figure 30. Calculated distribution of the surface charge density of a negative-polarity voltage pulse (charge distributions at 2 μs, $\varepsilon_r = 8$).

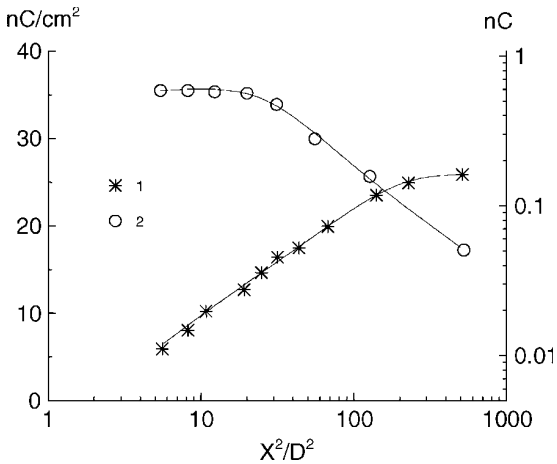

Figure 31. Calculated transferred charges of microdischarges (1) and surface charge density (2) depending on $(X/D)^2$ (X, inter-channel distance; D, microdischarge diameter).

channels is accompanied by short current impulses in the external circuit (figure 5). The field strength between the strips is far from the breakdown value (figure 29).

The extension of the charged area on the dielectric surface depends on the voltage amplitude. In figure 30 with negative polarity this value is several millimetres (in this figure charges of opposite polarity also appear because the movement of positive as well as negative ions has been considered). With positive polarity, the channel extension is considerably larger. With an ac voltage, the discharge extension is between that with positive and negative polarity (figure 10). The outer boundary of the charged area is determined by the first positive half-cycle of the applied voltage. For the succeeding negative half-period, the extension of the negative charged layer is enlarged by the outer positive charges on the surface, enhancing the field strength component parallel to the surface. It has been proved experimentally that with an ac voltage the outer region of the surface charge layer is charged positively [8].

4.2. Interaction of discharge pulses

Up to now the dynamics of separate microdischarges and single discharge steps on dielectric surfaces, respectively, have been discussed. However, the DBD consists of a multitude of such events, distributed in the discharge gap and on the surface of the dielectric, respectively. The value of the transferred charge of a microdischarge (or discharge step) multiplied by its number density per time and area unit (unit of electrode length) defines the discharge power density and is a measure of the intensity of the gas treatment.

The charge transfer through the discharge channel (step) is a complicated dynamic process as demonstrated previously. The resulting value of the transferred charge depends mainly on the dimensions of the discharge arrangement, on the specific capacitance and on the width of the discharge gap in VD arrangements. Other parameters are the pressure and type of process gas, especially its effective ionization coefficient. From experiments, it follows that an enlargement of the degree of electronegativity (e.g. from air to SF_6) decreases the diameter of the microdischarge channels and increases its number density in the VD case [21].

An increase in the specific capacitance increases the transferred charge (in the VD case, figure 7) and decreases the extent of the discharge (in the SD case, figure 11), respectively.

The transferred charge and the number density of channels affect the specific discharge power. They depend on one another. There is interference between adjacent channels resulting from the shielding effects. The closer the channels are the more pronounced are the interactions.

In figure 29 equipotential lines of discharge channels in a SD arrangement with positive polarity are shown. The distribution results from positive ions which are deposited on the dielectric surface in parallel strips. The farther apart these strips are the higher the field strength is between adjacent discharge channels and vice versa. The probability of new channels emerging in between adjacent ones increases as the field strength increases.

A similar mechanism for channel generation takes place in VD arrangements. If the inter-channel distance is infinity, the transferred charge of a single microdischarge will have a maximum value. Continually decreasing the inter-channel distance will result in a shielding effect from surface charges of adjacent microdischarges which, in turn, will reduce the power of the microdischarge development because of the reduced field strength. This behaviour has been confirmed by modelling the inter-channel interference (figure 31, [22]). The transferred charge of the microdischarges depends on $(X/D)^2$, X being the inter-channel distance and D the channel diameter (curve 1 of figure 31). This parameter is a measure of the size of the influence area of a microdischarge related to its cross section. At high values, the transferred charge reaches a saturation value and the microdischarges are no longer influenced by adjacent ones.

Curve 2 of figure 31 describes the surface charge density (transferred charge per unit of surface area) dependence on the same parameter. The charge density remains constant at high microdischarge number densities (short inter-channel distances) and decreases with increasing inter-channel distance. This decrease is somehow compensated for by the increase in the transferred charge at increasing inter-channel distances. At an inter-channel distance of less than four to five times the channel diameter ($(X/D)^2 < 16$–25), the surface charge density is constant. As the microdischarge

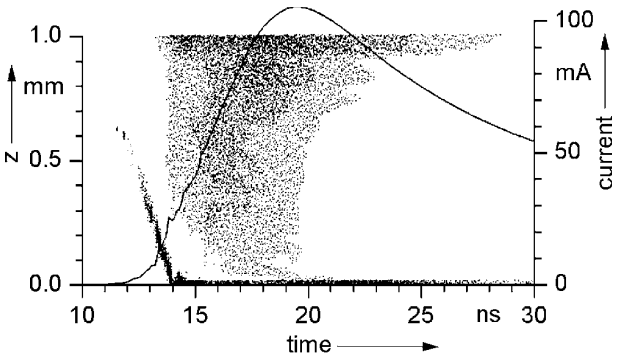

Figure 32. Streak-photograph and current of a single (VD) microdischarge (modelling results for $\varepsilon_r = 5$, thickness of the dielectric 2 mm and air at atmospheric pressure).

diameter in air at atmospheric pressure, a discharge gap of 1 mm and a relative permittivity of 5 is typically about 400 μm (and 1.2 mm at $\varepsilon_r = 50$), the inter-channel distance must be about 2 mm (and 6 mm, respectively). The corresponding microdischarge number densities are 8 and 1 cm^{-2}. These values have been obtained experimentally as well [23].

5. Energy density of the discharge

5.1. Charge transfer during a discharge pulse

The DBD is one of the most effective non-thermal plasma sources. It is characterized by an effective conversion of electric field energy to chemical or physical processes in gases or onto surfaces for many applications. On one hand, the efficiency is determined by the total amount of energy released in the discharge in general. On the other, the efficiency depends on the value of the field strength, which has to be adapted to the process under consideration. From this it follows that the effectiveness of a special application of DBDs crucially depends on the dynamics of charge transfer within the discharge.

The energy release is connected to a movement of charged particles, of electrons and ions. As the DBD is a non-equilibrium phenomenon, there is a significant gap between the mean energy of electrons and heavy particles. The mean electron energy in the discharge is about several eV, that of the heavy particles around 0.03 eV (∼300 K) at the conditions under consideration. While the energy of the electrons is utilized for chemical and physical purposes, the energy of the ions is, in general, useless.

The energy consumption in DBDs is combined with the movement of charge carriers, i.e. current. The energy release starts simultaneously with the development of the initial avalanche; however, a remarkable value is not reached until the appearance of the streamer in VD arrangements (figure 32, compare figure 2). The energy density (proportional to the darkness in figure 32) reaches its maximum value after cathode-layer formation and decreases again during charge accumulation on the dielectric.

During cathode-layer formation, the current density reaches a level in the order of a hundred A cm^{-2} (table 1). After cathode-layer formation and surface charge

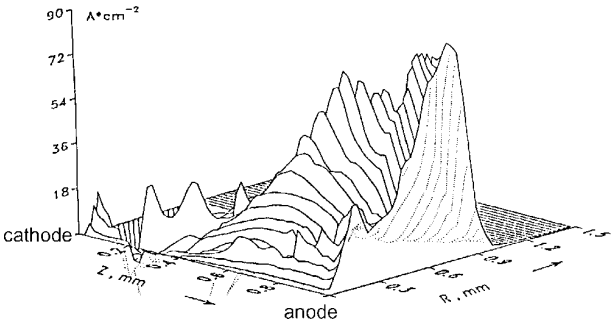

Figure 33. Calculated radial current density of a microdischarge at current maximum (air at atmospheric pressure, gas gap 1 mm, thickness of the dielectric 2 mm, $\varepsilon_r = 50$).

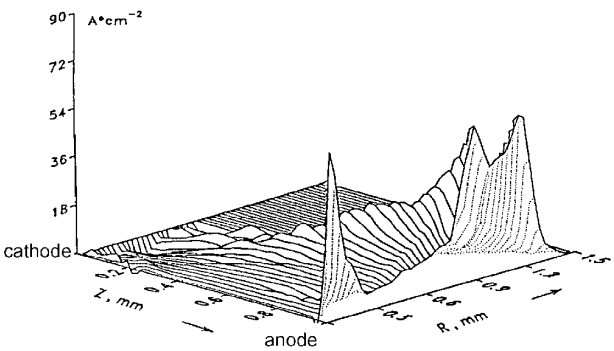

Figure 34. Calculated radial current density of a microdischarge at 6 ns after current maximum (conditions as in figure 33).

accumulation the main charge transfer and energy release are shifted to the peripheral region of the discharge channel at higher field strengths (figure 33). The radial boundary of the surface charge determines the position of the radial current density maximum. The maximum moves with expansion of the surface charge (figure 34).

In SDs with the boundary conditions under consideration, no cathode layer, in general, exists. This is an important difference between VDs and SDs. In the absence of an efficient source of secondary electrons, the current density is low, about 1 A cm^{-2}. In any case, a shielding effect caused by surface charges exists as well.

In SDs, the drift distance of electrons on the dielectric becomes longer with time (at each successive discharge step). The charge transfer process is shifted to a region with lower field strength where the effective ionization coefficient is negative. In any case, in SDs the charge transfer as well as the energy release are less intensive.

5.2. Energy density distribution

The main charge transport and energy release in the discharge channel (or step) takes place within 30–100 ns with the conditions under consideration. The power and energy density can be calculated if the field strength and electron density distributions are known (figure 35).

There are two maxima in the energy density distribution in the VD case: at the cathode layer and in the middle of the conductive channel (figure 35(a)). The first maximum is related to energy release in the cathode layer and refers to losses by positive ions. In the second, the energy

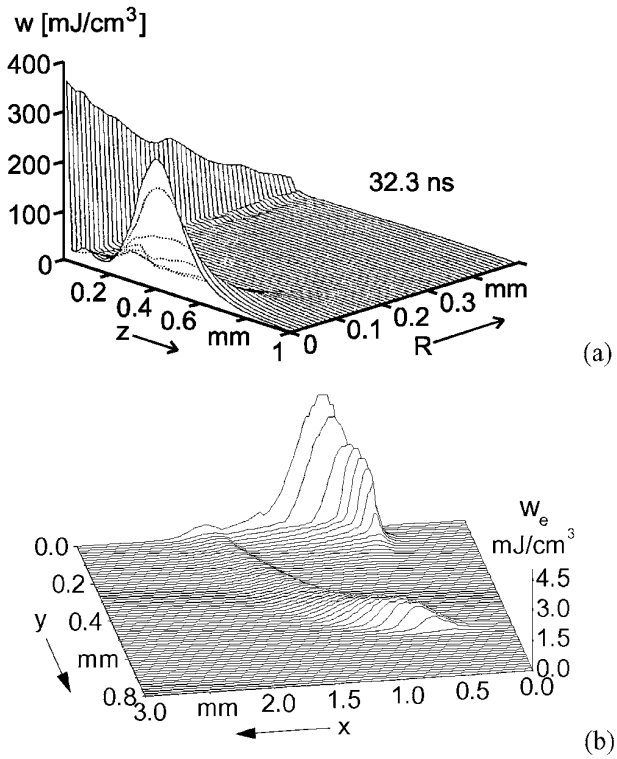

Figure 35. Energy density in the discharge region of (a) a VD and (b) an SD immediately after the current pulse ($\varepsilon_r = 5$, thickness of the dielectric 2 mm, air at 1 bar).

losses during the whole development of the discharge channel are accumulated during the first avalanche, streamer formation and propagation, as well as from the appearance of the cathode layer until extinction of the discharge. The displacement of the charge transfer to outer regions of the discharge channel does not affect the energy density distribution.

The less intensive processes in SDs lead to a broader spatial distribution of energy density with considerably lower values (figure 35(b)). In this case, the main energy losses take place in a layer near the dielectric surface with a thickness of about 100 μm.

The total amount of transferred charge and energy consumption by a single microdischarge in the VD case as well as the peak current are summarized in table 2 among others. The values depend mainly on the permittivity of the dielectric. The total energy loss and transferred charge of an SD is at least an order of magnitude smaller with comparable geometrical conditions.

5.3. Process efficiency of barrier discharge reactors

In most applications of DBDs, the discharge is utilized to excite internal states of atoms and molecules in order to obtain radicals, radiation or dissociated particles. Any internal state is characterized by a threshold or activation energy and the rate constant of the reaction. From the Arrhenius equation, it follows that the rate constant depends on the mean electron energy. This means that the rate constant rises exponentially as long as it is lower than the threshold energy and rises rather slower if it is higher. The mean electron energy is nearly

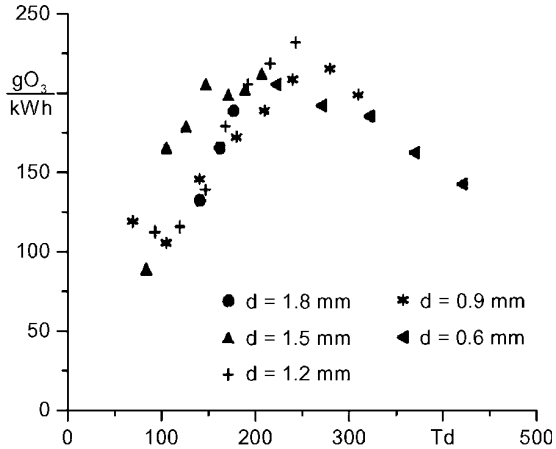

Figure 36. Measured values of ozone synthesis efficiency from oxygen [24].

proportional to the local electric field strength and in the case of air or oxygen at atmospheric pressure about 3–5 eV at breakdown conditions.

The reaction efficiency can be defined as the number of particles under consideration per unit of consumed energy, e.g. the number of UV photons produced in plasma display panels or the number of dissociated oxygen molecules for the ozone synthesis per unit of energy. In general the efficiency depends on several discharge parameters and has to be optimized. However, the parameters are not constant during the discharge development. In order to demonstrate the complex dependencies the production of ozone as a sequence of temporal and spatial events is taken as an example. Ozone synthesis has a comparatively simple 'chemistry' as long as the concentration is low. With this condition, the ozone yield is a measure of oxygen dissociation with a threshold energy of about 6 eV.

The measured values of the efficiency of ozone synthesis from oxygen are presented in figure 36 in dependence on the reduced electric field strength. The maximum is near the breakdown field strength. Unfortunately, the breakdown field strength can only be slightly influenced. However, there are some possibilities to tailor the discharge, e.g. by quenching the discharge at an early state or by exploiting the nonlinearity of the Paschen curve.

The mean field strength in the well conducting channel of a microdischarge (or a discharge step) depends mainly on nature of the gas and its pressure. Its value is near to the level at which the effective Townsend ionization coefficient is zero (at about 100 Td). For air or oxygen, the mean field strength has about half the value of the breakdown field strength. For oxygen, this means the efficiency must be around 100 gO_3 (kW h)$^{-1}$ (figure 36). Actually the efficiency of optimized industrial ozone generators is not far from 200 gO_3 (kW h)$^{-1}$ at low concentrations.

If one takes into account the temporal development of the charge transfer process, it is obvious why the efficiency can be higher than 100 gO_3 (kW h)$^{-1}$ in oxygen. Initially electrons move through the gas with an electric field strength near the breakdown level and the efficiency is maximal (figure 37 and 36). In VDs, the mean electric field strength drops (as well as the efficiency) simultaneously with cathode-layer

Table 2. Parameters of discharge channels in VD arrangements (conditions as in figure 35).

Relative permittivity	Transferred charge (nC)	Peak current (mA)	Number of O atoms	Total energy (μJ)	Current density (A cm^{-2})
5	0.81	102	2.0×10^{12}	5.5	65
50	4.60	620	8.7×10^{12}	24.7	65

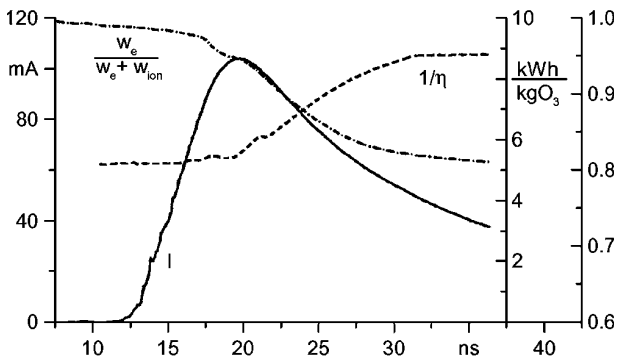

Figure 37. Current, related electron energy consumption and reverse value of ozone efficiency during the development of a microdischarge (VD arrangement, oxygen at 1 bar, discharge gap 1 mm, $\varepsilon_r = 5$).

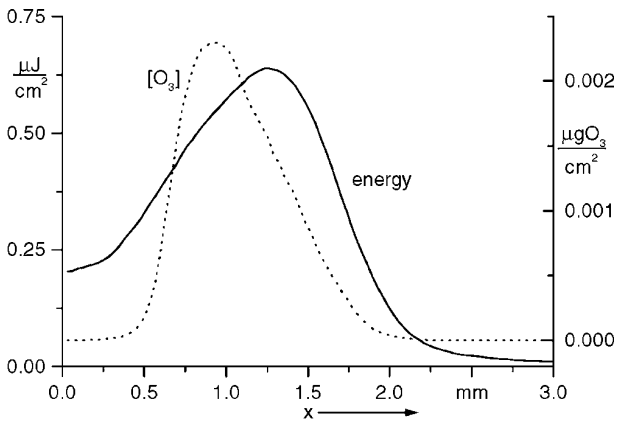

Figure 38. Distributions of electron energy consumption and ozone (oxygen atom) of a SD related to the unit of dielectric surface area (oxygen, 1 bar, $\varepsilon_r = 5$).

formation and the development of the conduction channel. The energy losses double and the inverse efficiency reaches a value of 9 kW h kgO$_3$$^{-1}$ or 110 gO$_3$ (kW h)$^{-1}$ (figure 37). This corresponds to field strengths of about 100–110 Td in the conduction channel (figure 36). This very value has been found in the conductive channel (figure 26(a)), where most of the energy is consumed (figure 35).

The DBD in SD arrangements is less intensive. In general, no cathode layer exists with the conditions under consideration; the current density is smaller. The electrons move in a region of decreasing field strength. During surface charge accumulation, the field strength is modified. Its mean value nearly reaches the level of that in well-developed channels in VD arrangements. This means that in SDs the efficiency must be roughly similar to that in VDs. During a discharge step, from ignition to extinction, the variation in the efficiency is less pronounced, it drops about 30% only.

There is another difference between SD and VD behaviour. In VD arrangements, the energy density distribution practically coincides with the oxygen atom distribution, except for the cathode-layer region. The nonlinear initial conditions during discharge development of SDs cause a shift between these two distributions (figure 38). The current flows between the electrode and the dielectric surface. During the flow the electric field strength (and hence the mean electron energy) changes over a wide range. Near the electrode the field strength is comparatively high and the oxygen atom production is effective, farther from the electrode it becomes less effective; at the farthest tip the electron energy is too low to dissociate. This is why there is a discrepancy in the distributions of energy loss and oxygen atom concentration.

The overall reaction efficiency is the result of a sequence of processes, which start the moment the initial electrons appear and end with discharge extinction. Although this chain of spatial and temporal events is quite different in VD and SD arrangements, they lead approximately to the same results. For example, ozone synthesis from oxygen with VDs and SDs has nearly the same efficiency. This looks strange, because the initial field strength distributions and discharge dynamics are quite different. The explanation is as follows. During the discharge development, which starts from different initial conditions, well-developed discharge regions with nearly the same electric field strengths (figures 17(b) and 26(a)) appear in both cases. The main energy consumption happens in these conductive regions. In the VD case the electric field strength decreases during the formation of the conductive channel from the initial breakdown level to the equilibrium one, this is about 100 Td for oxygen. In the SD case, the initial decreasing field strength distribution increases at the tip of the propagating discharge leading to a conductive region with field strength at about equilibrium level (figure 26(a)). That is why in both arrangements the energy consumption occurs at comparable conditions and the efficiency of ozone synthesis is similar.

6. Conclusions

The DBD is characterized by a dielectric layer between the electrodes. The dielectric layer prevents the occurrence of a high current, constricted discharge channel. Charge carriers accumulate locally on the dielectric surface and hence quench the discharge development at an early stage. That is why the DBD in air and oxygen at atmospheric pressure consists of numerous microdischarges in VD arrangements, which consist of columns and surface discharges on the dielectric, and a discharge layer on the dielectric in SD arrangements, respectively. The surface discharge patterns in both arrangements are comparable. If the dielectric is the cathode, the surface discharge comprises of channels, with opposite polarity the discharged area is uniform.

On increasing the voltage the number of microdischarges increases in the VD case. In the SD arrangement an increasing voltage causes a stepwise growth of the discharged area (discharge steps). The size of this area depends, apart from the voltage amplitude, on the polarity and the specific capacity of the dielectric.

The duration of a microdischarge (or discharge step) is of the order of a few 10 ns at atmospheric pressure. The transferred charge during this event is well reproducible in electronegative gases and the VD case. It depends on the dimensions of the configuration and the specific capacity of the dielectric.

While the current–voltage characteristic is mainly linear in the VD case, it is nonlinear for SD arrangements. This is explained by the growth of the discharged area (or capacity) with voltage.

The burning voltage of DBDs is considerably influenced by the surface charge density resulting from the preceding discharges with an ac supply. The density depends on the specific capacity of the dielectric and its maximum value is between 10–100 nC cm^{-2}. The (micro-)discharge behaviour is characterized by an initial phase of electron multiplication within an undisturbed electric field, a phase of high conductivity with the occurrence of a cathode layer and finally an extinction phase. The highly conductive phase is initiated by a cathode-directed ionizing wave (or streamer). Its development is ruled by photoemission and attachment–detachment processes. Photoemission is important during the initial phase of the discharge development, later on the dominant source of secondary electrons is electron emission by positive ions. The initial phase of the discharge is about an order of magnitude longer than the measured duration if photoemission is omitted.

A distinct cathode layer appears only if the discharge process is well developed. Depending on construction of the discharge arrangement and gas properties, the discharge process can be quenched early. In this case the field strength in front of the cathode may reach values in between the initial one and that of a well-developed cathode layer. This means in certain circumstances that the discharge may be quenched before cathode-layer formation.

In general the cross section of the (normal) cathode layer is defined by its specific capacitance. As the current density of the layer is constant, the discharge current is determined by the cross section of the cathode layer. It grows with the radial expansion of the layer and reaches its maximum at its maximum size.

The field strength distribution has a maximum in the cathode layer and an almost constant value in the conductive channel, which is nearly frozen after the appearance of the cathode layer. The constant value of the field strength in the conductive channel is determined by the equilibrium between electron generation and loss processes. In air and oxygen at atmospheric pressure it is about 100 Td.

In any configuration the DBD has a certain spatial structure; it consists of a series of microdischarges (VD) or discharge steps (SD). The interaction between surface charges and charge carrier flow in the gas region determines the density of the discharge patterns on the dielectric surface.

The development of the resulting discharge patterns, which takes place at the same polarity of applied voltage, depends on the discharge arrangement (VD or SD). In the VD case microdischarges leave behind charged spots on the dielectric surface, which decrease the mean field strength at this location. During the following voltage increase, microdischarges will emerge at other locations where the surface charge density is at a minimum. In the SD case an increasing voltage causes an increase in the discharge area on the dielectric surface.

The microdischarge (discharge step) density on the dielectric surface depends on the value of the transferred charge. In the VD case, a higher value for the charge transferred through the discharge channel means that a smaller channel density is detected on the dielectric surface. In the SD case the discharge channel density (for positive polarity) seems to be constant. Transferred charge enlargement increases the length of the discharge area on the dielectric surface only.

The discharge current reaches a maximum after cathode-layer formation in the VD case. That is why the main charge transfer and energy release takes place after cathode-layer formation.

The energy release is not homogeneously distributed within the discharge region. In general (at least for ozone synthesis) the field strength at the position of maximum energy density is significantly lower than the most effective one for the process under consideration. Apart from the energy density maximum in the discharge column an additional maximum has been found in the VDs cathode layers. This maximum mainly results from the movement of ions. In SDs a 'normal' cathode layer does not appear for the boundary conditions under investigation.

The microdischarge (discharge step) energy density is comparatively low. The resulting temperature jump in the discharge region is estimated to be in the order of a few Kelvin after the termination of the microdischarge (discharge step).

The energy conversion from electric field to the desired process (e.g. production of UV radiation or ozone) takes place in the DBDs conductive region. Electron collisions are more effective at high field strength, i.e. in the early phases of discharge development. Late phases cause a remarkable energy release by ion movement, which means a considerable increase in losses and a corresponding increase in energy consumption. To improve efficiency the discharge has to be quenched in an early phase of its development.

Acknowledgments

The authors gratefully acknowledge the financial support of the German Research Association (DFG) as well as that of the Russian Fund of Basic (Fundamental) Research (RFFI) for some of the investigation.

References

[1] Tanaka M, Yagi S and Tabata N 1982 The observation of silent discharge in air, oxygen and nitrogen by super high sensitivity camera *Trans. IEE Japan* A **102** 533–40 (in Japanese)

[2] Eliasson B, Hirth M and Kogelschatz U 1987 Ozone synthesis from oxygen in dielectric barrier discharges *J. Phys. D: Appl. Phys.* **20** 1421–37

[3] Eliasson B and Kogelschatz U 1991 Modelling and application of silent discharge plasmas *IEEE Trans. Plasma Sci.* **19** 309–22
[4] Braun D, Küchler U and Pietsch G J 1991 Microdischarges in air-fed ozonizers *J. Phys. D: Appl. Phys.* **24** 564–72
[5] Braun D, Gibalov V I and Pietsch G J 1992 Two-dimensional modelling of the dielectric barrier discharge in air *Plasma Sources Sci. Technol.* **1** 166–74
[6] Neiger M 1992 Dielectric barrier discharges: an unusual new light source *Proc. Science and Technology of Light Sources (LS6) (Budapest)* ed L Bartha and F J Kedves, pp 75–82
[7] Steinle G, Neundorf D, Hiller W and Pietralla M 1999 Two-dimensional simulation of filaments in barrier discharges *J. Phys. D: Appl. Phys.* **32** 1350–6
[8] Richter R and Pietsch G 1995 Discharge phenomena on a dielectric surface with extended electrodes *Proc. 11th Int. Conf. on Gas Discharges and Their Applications* vol 2, pp 280–3
[9] Murata T, Okita Y and Terai K 1997 Distribution of surface discharge for ozone generation *Proc. XXIII Int. Conf. on Phenomena in Ionized Gases (Toulouse)* vol III, pp 82–3
[10] Boeuf J-P, Punset C, Hirech A and Doyeux H 1997 Physics and modeling of plasma display panels *J. Physique* **IV** C4 3–14
[11] Pietsch G J and Gibalov V I 1997 Discharge phenomena on a dielectric surface with extended electrodes *Proc. 12th Int. Conf. on Gas Discharges and Their Applications* vol 2, pp 750–7
[12] Samoilovich V, Gibalov V and Kozlov K 1997 *Physical Chemistry of the Barrier Discharge* 2nd edn (Düsseldorf: DVS)
[13] Kogelschatz U, Eliasson B and Egli W 1997 Dielectric barrier discharges—principle and applications *J. Physique* **IV** C4 47–66
[14] Pietsch G J, Braun D and Gibalov V I 1993 Modeling of dielectric barrier discharges *Non-Thermal Plasma Techniques for Pollution Control (NATO ASI Series Part A)* vol 34, ed B M Penetrante and S E Schultheis, pp 273–86
[15] Müller S and Zahn R-J 1996 On various kinds of dielectric barrier discharges *Contrib. Plasma Phys.* **36** 697–709
[16] Heuser C and Pietsch G 1980 Prebreakdown phenomena between glass–glass and glass–metal electrodes *6th Int. Conf. on Gas Discharges and Their Applications (Edinburgh) IEE Conf. Publ.* **189** 98–101
[17] Drimal J, Gibalov V and Samoilovich V 1987 Silent discharge in air, nitrogen and argon *Czech. J. Phys.* B **37** 641–4
Drimal J, Gibalov V and Samoilovich V 1987 The magnitude of the transferred charge in the silent discharge in oxygen *Czech. J. Phys.* B **37** 1248–55
[18] Sigmond R S 1979 Gas discharge data sets for dry oxygen and air *Report* Norges Tekniske Hogskole, Trondheim
[19] Eliasson B and Kogelschatz U 1986 Basic data for modelling of electrical discharges in gases: oxygen *Brown Boveri Research Report* KLR 86-11 C
[20] Francis G 1956 The glow discharge at low pressure *Encyclopedia of Physics* vol XXII (Gas Discharges II), ed S Flügge (Berlin: Springer)
[21] Bertein E H 1973 Charges on insulators generated by breakdown of gases *J. Phys. D: Appl. Phys.* **6** 1910–16
[22] Gibalov V I and Pietsch G 1994 Energy release in a microdischarge channel *Russ. J. Phys. Chem.* **68** 1023–8
[23] Bagirov M A, Nualiev H A and Kurbanov M A 1972 Investigations on a discharge in an air gap limited by a dielectric and method of determining the number of partial discharges *J. Tech. Phys.* **43** 629–34 (in Russian)
[24] Gibalov V I 1994 Synthesis of ozone in a barrier discharge *Russ. J. Phys. Chem.* **68** 1029–33